Thermophysics and Aeromechanics, *2022*, *Vol. 29*, *No. 1*

DOI: 10.1134/S0869864322010024

Modeling of unsteady subsonic flow around an axisymmetric body with a turbulator*

I.A. Shirokov and T.G. Elizarova

Keldysh Institute of Applied Mathematics of the RAS, *Moscow*, *Russia*

E-mail: ivanshirokov@inbox.ru

(*Received August 4*, *2021*; *revised September 17*, *2021*;
accepted for publication October 20, *2021*)

The results of numerical simulation of external subsonic unsteady flow around an axisymmetric model are presented. The simulation uses a quasi-gas-dynamic algorithm implemented on an unstructured tetrahedral grid. A turbulator in the annular flap shape is allocated on the model surface: it sets the position of a laminar-turbulent transition. The problem statement corresponds to experiments for this model placed in a wind tunnel. The overall flow pattern, the distribution of the pressure coefficient on the surface, and the turbulent pulsation parameters demonstrate fair qualitative and quantitative agreement with the experimental data.

Keywords: quasi-gas-dynamic (QGD) equations, subsonic flow, laminar-turbulent transition.

Introduction

The papers [1, 2] presented experimental results of the research for flow past an axisymmetric model in a wind tunnel at subsonic flow modes. The general view of this model is shown in Fig. 1. This study was focused on estimating the velocity pulsation originating to laminar-turbulent transition in the separation flow: the surface flow was visualized. Few experimental tests dealt with a wire-shaped turbulator which is stretched across the model.

Simulation of flow separation from a smooth surface is a challenging task because the exact position of laminar-turbulent transition is not fixed. In some experiments, an annular bump on a smooth body surface was arranged: this assigns the position of flow separation. In the present paper, the simulation of separation phenomenon and laminar-turbulent transition is performed using the Quasi-Gas-Dynamic (QGD) algorithm [3 – 6]. Here, a special form of artificial viscosity works as turbulent dissipation; this is a difference between the QGD equations and the Navier–Stokes equations.

Previously, the QGD algorithm was an instrumental tool for simulation of subsonic flows [7, 8] and supersonic flows [9, 10]. This approach was efficient in simulation of laminar-turbulent transition in a compressible gas flow: the examples are the problem of Taylor–Green

* Research was financially supported by the Russian Science Foundation, Project No. 19-11-00169.

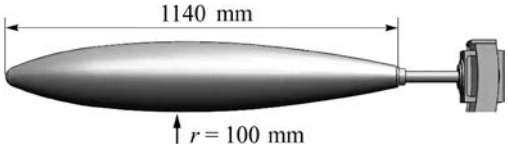

Fig. 1. General layout of the model.

vortex decay [7] and the problem of Couette turbulent flow [8]. Both examples of simulation demonstrated a compliance with basic computational and experimental data both in metrics of kinetic energy dissipation (vortex decay) and in magnitude of velocity pulsations (Couette flow).

The authors apply the QGD algorithm for simulating a turbulent gas flow where the turbulence is induced by a turbulator on the axisymmetric body (Fig. 1). The flow parameters meet the experimental conditions from [1]: freestream velocity U_0 = 10 m/s, Mach number M = = 0.0294, Reynolds number (calculated from size of 1 m) is Re = 630000, and the attack angle is 4°. Here we take the gas constant R = 287 J/(kg·K), specific heat ratio is γ = 7/5, sound speed in the freestream is 340 m/s.

The previous experiments with CFD of the flow around an axisymmetric body demonstrated that the flow pattern and position of flow separation point strongly depend on the accuracy of body shape approximation and quality of computation grid [11]. The mesh based on cells with a regular shape is preferable for CFD: this gives an accurate approximation of macroscopic equations on this type of grid. The research [12] described a rather universal algorithm for constructing an approximately uniform grid over the surface of any axisymmetric model. In this case, the shape of surface cells is close to square, and the body geometry is reproduced with a high accuracy. The approach is as follows. After the on-surface grid is constructed, we can create an irregular tetrahedral mesh in the space around the model using the mesh generator TetGen [13]. The near-surface cells in the spatial grid are close to regular tetrahedral geometry. This approach was used in this research. The special grid parameters are the following: total number of points is 933838, the number of tetrahedral cells is 5503321, the number of points on the surface model is 93576, and the number of triangle cells over the model surface is 187148. The typical size of the surface cell is 0.004 m (in paper [12], this parameter was denoted as Step). The grid generation was performed within a Cartesian coordinate system (x, y, z) with the x-axis along the model symmetry axis, and the coordinate origin coincides with the front end.

Figure 2*a* presents a general outlay of the grid in the cross section z = 0 (the freestream velocity vector is in the same cross section) and the turbulator position is indicated. Figure 2*b* illustrates a fragment of the grid near the nose part of the model, and the relatively regularly shaped cells are visible near the surface.

The generation of a grid with almost-regular tetrahedral cells in the boundary layer improves the approximation of macroscopic equations. In turn, this offers an option of computing with a low value of additional viscosity, but at a higher Courant number (0.5). This results in a developed pattern of flow separation and laminar-turbulent transition after a moderate computation time.

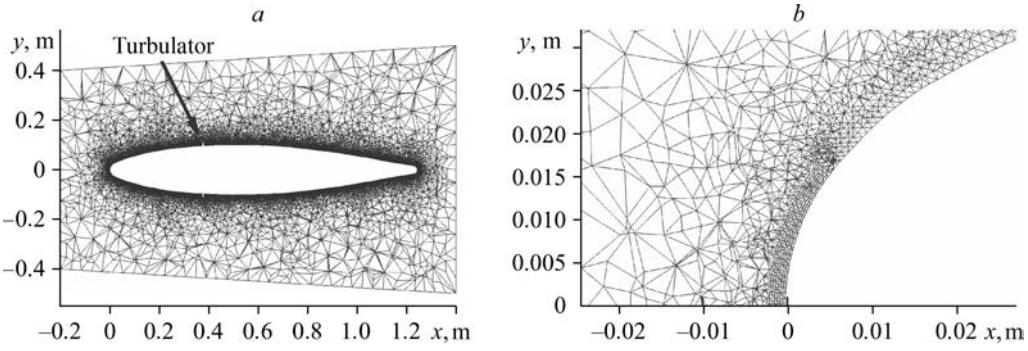

Fig. 2. General outlay of the grid (*a*) and a piece of grid for the nose part (*b*) for cross section z = 0.

The turbulator is an annular bump on the model surface placed in the cross section with $x = 0.374$ m (data taken from [2]). The turbulator thickness is about 0.005 m and its height is 0.02 m.

Mathematical model and numerical solution method

The external subsonic flow past a body was simulated using a set of quasi-gas-dynamic equations for ideal polytropic viscous gas (the approach was developed in [3 – 5]). Here we take the QGD equations for simulation in the format presented in [9, 12]. The key gasdynamic parameters are gas density, three components of velocity, and pressure. The temperature is defined from the ideal gas equation of state. The energy per gas volume unit is defined as a sum of kinetic and internal energy. The simulation of subsonic flow needs a knowledge of the shear viscosity μ in the form of temperature dependency:

$$\mu = \mu_0 (T / T_0)^{\omega}, \tag{1}$$

where μ_0 is the gas viscosity for the free stream at T_0, $\omega = 0.74$ is the exponent for intermolecular interaction. The thermal conductivity coefficient is calculated from the ratio:

$$\kappa = \mu / (\mathrm{Pr}\,(\gamma - 1)), \tag{2}$$

where Pr = 0.737 is the Prandtl number. The bulk viscosity coefficient taken in approximation format takes the form:

$$\varsigma = \mu((5/3) - \gamma)\,. \tag{3}$$

The coefficient τ (defining the additional dissipation for QGD algorithm) for the case of viscous polytropic gas is about of the free time between the collisions of gas particles. In the presented computations, this coefficient is related to the spatial cell size h through the ratio:

$$\tau = \alpha h / c, \tag{4}$$

where c is the local speed of sound, and $\alpha = 0.05$ is an adjustment parameter.

This type of artificial viscosity is instrumental in simulation of a subsonic turbulent flow using a single adjustment parameter α.

For computations on an irregular tetrahedral mesh we used an improved software complex [14] suitable for simulating of unsteady viscous gas flows for the case of external flow around a body with arbitrary shape (using the QGD algorithm). This software uses the gasdynamic parameters in dimensionless form. The following dimensional parameters were taken: characteristic length $L_0 = 1$ m, gas density ρ_0, and the speed of sound c_0 for the free stream. The gas state equation of state in dimensionless form is written as $p = \rho T / \gamma$, speed of sound $c_0 = \sqrt{T}$, Mach number $\mathrm{M} = U_0 / c_0$, the Reynolds number $\mathrm{Re} = \rho_0 U_0 L_0 / \mu_0$, the coefficient of molecular shear viscosity $\mu = (\mathrm{M} / \mathrm{Re}) T^{\omega}$. The finite-difference approximation for macroscopic QGD equations is constructed using the control volume method. Since all dissipation coefficients depend on the local parameters, the tetrahedral grid provides the first order approximation in space.

At the initial time, the inlet boundary has the parameters from the free stream. Inside the computational domain, we assign the same parameters except the gas velocity: gas is motionless at zero time. These initial conditions in dimensionless format are the following:

$$\rho = 1,\ T = 1,\ p = 1/\gamma.$$

Since we deal with subsonic flow past a body, the boundary conditions are as follows [4, 12]. The solid boundary of the body has the no-slip condition (velocity vector is zero) and we apply

the additional condition from the QGD algorithm: normal derivatives for pressure and density on the solid wall equal zero (solid boundary has adiabatic conditions). The values of velocity and density at the inlet boundary are kept constant. The normal derivative for pressure is also zero at the inlet boundary. The temperature for inlet boundary is calculated from the gas equation of state. This boundary condition has non-reflecting nature and allows upstream spreading of disturbances.

The drift conditions for velocity are assigned at the outlet and lateral boundaries (normal derivatives are zero). The pressure at the outlet and lateral boundaries is constant and equal to the initial pressure for the undisturbed free stream. The temperature is defined by the equation of state. The outlet boundary conditions are non-reflecting and allow downstream spreading for disturbances.

The solution of the described problem for the mesh analogs of QGD equations (with account for relations (1) – (4)) can be found using an explicit difference scheme with the first order of approximation in time. The time step is calculated as $h_t = \beta h / c \approx 9 \cdot 10^{-8}$ s, where $\beta = 0.5$ is the Courant number, h and c are the local parameters described in (4).

Computations were performed at the K-100 supercomputer available in the Collective Exploit Center at Keldysh IAM of RAS [15]. The parallel computations technique was used based on the decomposition of the computational domain using the MPI standard and the METIS library and 128 processor cores were involved simultaneously. Hereby we present the computations of flow up to 0.26 s of dimensional time (equivalent to 87 units of dimensionless time). This takes about $3 \cdot 10^6$ iterations.

Pattern of separation flow and vortex generation

Figures 3 and 4 present the distributions of pressure coefficient $C_p = 2(p - p_0)/(\rho_0 U_0^2)$ (in dimensionless variables, $C_p = 2(p - 1/\gamma)/\mathrm{M}^2$) for the cross sections $z = 0$ and $y = 0$.

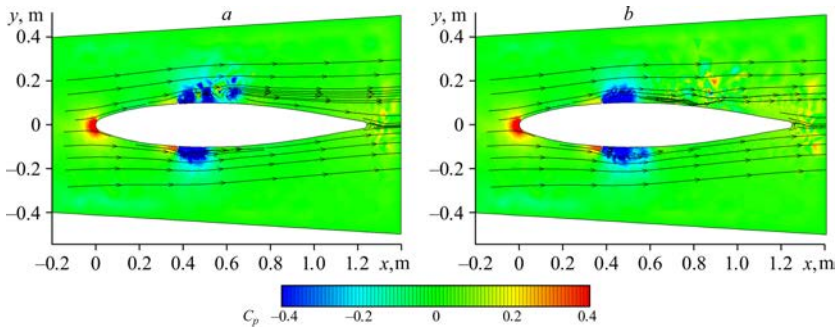

Fig. 3. Flow patterns at $z = 0$ for time $t = 0.095$ s (*a*) and $t = 0.155$ s (*b*).

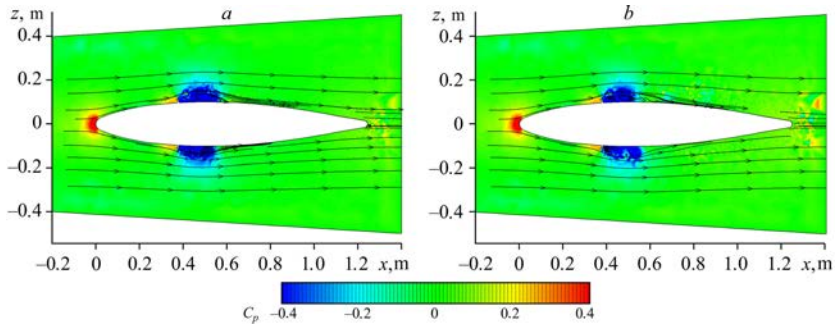

Fig. 4. Flow pattern at $y = 0$ for time $t = 0.095$ s (*a*) and $t = 0.155$ s (*b*).

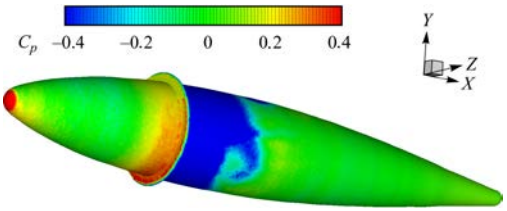

Fig. 5. Pressure coefficient over the surface.

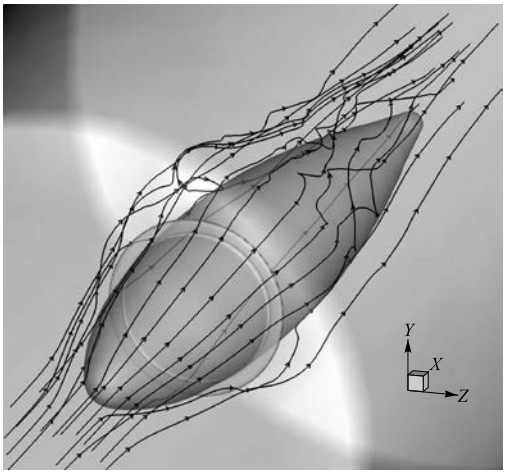

Fig. 6. Spatial streamlines near the body surface.

The flow lines are plotted in these figures. Figures 3*a* and 4*a* show the patterns at times $t =$ $= 0.095$ s (when the turbulent flow zone has been formed), and Figs. 3*b* and 4*b* describe time $t = 0.155$ s. Besides, the plots indicate the elevated pressure areas at the nose end (the pressure coefficient is about one unit) and ahead the turbulator. One can see a low pressure zones downstream the turbulator where the vortex-type separation flow is generated. Comparison of flow patterns at different time moments demonstrates the unsteady nature of flow. Comparison of flow patterns for cross sections $z = 0$ and $y = 0$ demonstrates the significantly 3D features of vortex flow downstream the turbulator.

Figure 5 shows the distribution of pressure coefficient over the model surface at time $t = 0.095$ s. One can see the zone of low pressure downstream the turbulator and asymmetric zone of high pressure due to non-zero angle of attack. The value of C_p at the model surface varies from 1.1 (a jump in the nosal zone) down to -0.7 (behind the turbulator). The tail part of the model at $x > 0.6$ indicates the variation in C_p from -0.1 to 0.1. For qualitative comparison of values C_p with experimental data we should note that research [2] was performed for the distribution of C_p in the boundary layer within the symmetry plane obtained in the wind tunnel at $U_0 = 16$ m/s and the zero angle of attack without turbulator. Experimental values for C_p vary from -0.2 to 0 at $x > 0.3$, i.e., without considering the pressure jump in the front part. Therefore, the simulated pressure coefficient is close to experimental data by the order of magnitude.

Figure 6 demonstrates the spatial streamlines near the body surface for time $t = 0.155$ s and vortex flow pattern is obvious.

The flow lines in a boundary layer and mapping of pressure coefficient on the surface for parameters $z = 0$, $t = 0.095$ s are shown in Fig. 7. The size of the separation zone (Fig. 7) is close to the experimental size. For qualitative comparison, Figure 8 presents a typical visualization of streamlines obtained in a wind tunnel at $U_0 = 20$ m/s and attack angle of 20° [2]. In this situation, the turbulator in experiments was placed at the same position as in our simulation configuration.

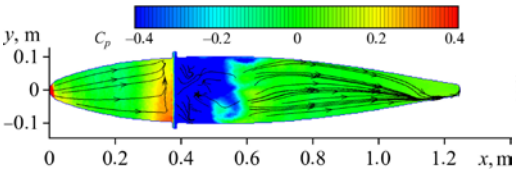

Fig. 7. Flow lines and levels of C_p in the boundary layer, obtained through simulation.

Fig. 8. Visualization of flow lines in the boundary layer (experiment).

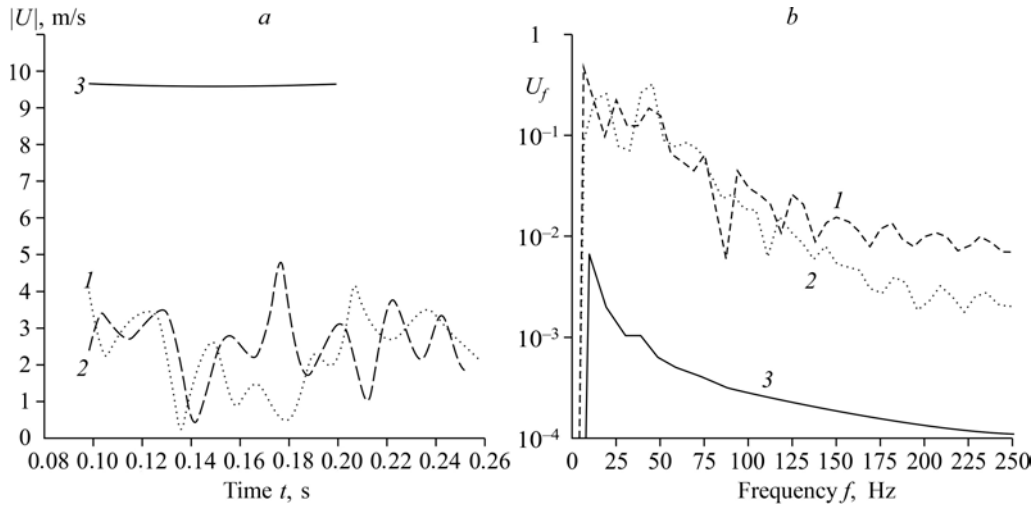

Fig. 9. Evolution of velocity module (left) and its spectrum (right) for three selected points.
1 — $x = 0.45$, $y = 0.12$, $z = 0$ m, *2* — $x = 0.45$, $y = 0$, $z = -0.12$ m, *3* — $x = 0.3$, $y = 0$, $z = -0.12$ m.

Time evolution of parameters and pulsation spectra

Figures 9 and 10 demonstrate the profiles for velocity and pressure coefficient as a function of time for three near-surface points with coordinates (in meters) shown in format (x, y, z). Two points were chosen behind the turbulator: (0.45, 0, –0.12), (0.45, 0.12, 0). The third point (0.30, 0, –0.12) is upstream the turbulator. Figure 9*a* demonstrates the developed oscillation of velocity at two points behind the turbulator (curves *1* and *2*) and almost zero oscillation upstream the turbulator (curve *3*). The corresponding spectra of velocity amplitude pulsation calculated through the Fourier discrete transformation are shown in Fig. 9*b*.

Similar to Fig. 9, Fig. 10*a* depicts the developed oscillations of pressure coefficient behind the turbulator (curves *1* and *2*) and almost zero oscillation upstream the turbulator (curve *3*). One can see the low-power oscillations that decay up to the time $t \approx 0.16$ s; this is due to the influence of initial conditions. Figure 10*b* presents the profiles of three components of velocity for the point (0.45, 0, –0.12) behind the turbulator.

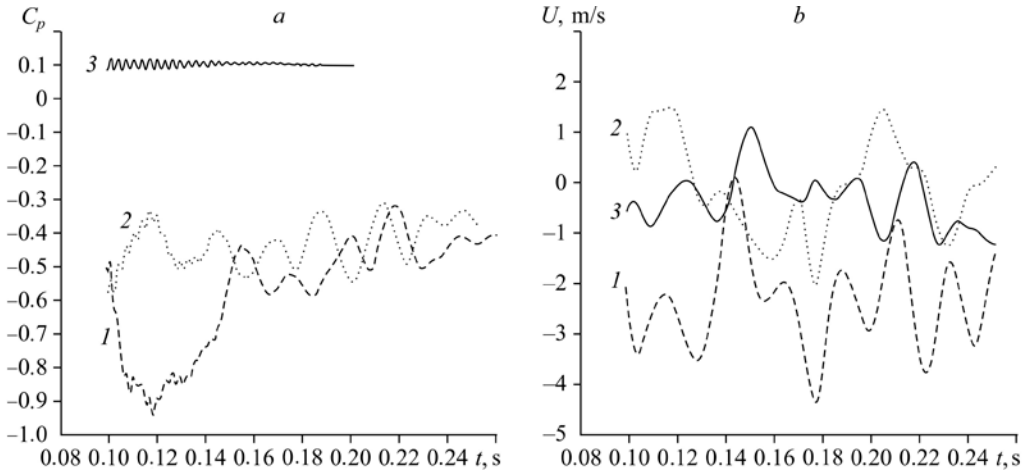

Fig. 10. Evolution of C_p (*a*) and velocity components (*b*).
a: *1* — $x = 0.45$, $y = 0.12$, $z = 0$ m, *2* — $x = 0.45$, $y = 0$, $z = -0.12$ m, *3* — $x = 0.3$, $y = 0$, $z = -0.12$ m;
b: profiles for velocity components U_x (*1*), U_y (*2*), U_z (*3*) for the point $x = 0.45$, $y = 0$, $z = -0.12$ m.

Table

Characteristics of velocity pulsations

Coordinates for U x, y, z, m	$\|U\|^{m}$ (average), m/s	$\|U\|'$ (pulsation), m/s	Characteristic frequencies, Hz
0.3, 0, –0.12	9.616	0.01034	25
0.45, 0, –0.12	2.631	0.8332	25, 50
0.45, 0.12, 0	2.348	0.9552	25, 50
Experiment	0 – 10	0.01 – 1.5	25, 50, 100, 150

The Table presents the characteristics of pulsations produced by CFD for three selected points. These are the average modulus of velocity $|U|^{m}$, the r.m.s. of pulsations $|U|'$, and the characteristic oscillation frequencies. For the sake of comparison, we present in this table the experimental values for velocity pulsations in the near-wall layer (for the same conditions: U_0 = 10 m/s, Re = 630000, attack angle 4°), but without turbulator [1]. Since the presented study offers the distributions of pulsation-related parameters over the entire surface of the body and their profiles in the normal directions, here the table presents only the top and minimum limits of experimental values for the same parameters (along with characteristic frequencies).

The conclusion can be drawn from data in Figs. 9, 10 and table data that the zone behind the turbulator (at x = 0.45 m) produces the oscillations with the r.m.s. velocity pulsation $|U|'$ about 1 m/s. This is close to the same value of pulsations in the near-wall layer obtained in experiments [1]. The simulated frequencies of flow oscillations (low-frequency range) are similar to those obtained in experiments [1]. The experimental high frequencies cannot be reproduced in simulation. Note that there are practically no oscillations upstream the turbulator (for x = 0.3).

Conclusion

The results of numerical simulation of subsonic flow past an axisymmetric body equipped with a turbulator demonstrated the possibilities of applying the QGD algorithm for studying the laminar-turbulent transition (observed in experiments with flow past a body). We observe a satisfactory qualitative agreement for distribution of pressure coefficient over the surface and quantitative agreement of turbulent pulsation parameters with experimental data. The QGD algorithm is instrumental for simulation of laminar-turbulent transition occurring without tools for flow turbulization, such as random disturbance of flow pattern, Tollmien–Schlichting waves or introduction of forced oscillation.

References

1. **A.V. Dovgal, B.Yu. Zanin, and A.M. Sorokin,** Stability of the laminar flow on a body of revolution at incidence, Thermophysics and Aeromechanics, 2014, Vol. 21, No. 4, P. 401–406.
2. **B.Yu. Zanin, A.V. Dovgal, and A.M. Sorokin,** Visualization of boundary layer separation on an axisymmetric body, AIP Conference Proceedings, 2018, Vol. 2027, P. 030131-1–030131-4.
3. **B.N. Chetverushkin,** Kinetic Schemes and Quasi-gas Dynamic System of Equations, CIMNE, Barselona, 2008.
4. **T.G. Elizarova,** Quasi-Gas Dynamic Equations. Springer, Dordrecht, 2009.
5. **Yu.V. Sheretov,** Regularized Equations in Fluid Dynamics, Tver State University, 2016.
6. **T.G. Elizarova and I.A. Shirokov,** QGD Equations and Examples of Applications in Gas Dynamic Flow Simulation, MAKS Press, Moscow, 2017.
7. **I.A. Shirokov and T.G. Elizarova,** Simulation of laminar–turbulent transition in compressible Taylor–Green flow basing on quasi-gas dynamic equations, J. Turbulence, 2014, Vol. 15, Iss. 10, P. 707–730.
8. **.A. Shirokov and T.G. Elizarova,** Application of quasi-gas dynamic equations to numerical simulation of near-wall turbulent flows, Computational Mathematics and Modeling, 2017. Vol. 27, Issue 1, P. 37–59.
9. **A.S. Epikhin and T.G. Elizarova,** Numerical simulation of underexpanded supersonic jets impingement on an inclined flat plate, Thermophysics and Aeromechanics, 2021, Vol. 28, No. 4, P. 479–486.

10. I.A. Shirokov and T.G. Elizarova Computational experiment in the problem of supersonic flow around a blunt body with tail expansion, Mathematical Modeling, 2020. Vol. 12, No. 3, P. 433 – 444.

11. I.A. Shirokov, Study of features of a subsonic flow past an axisymmetric model using QGD equations, Coll. of papers Conf. "Lomonosov Lectures". Section "Computational Mathematics and Cybernetics", April 15 –25, 2019. Publ. CS MSU department. MAKS Press, Moscow, 2019. P. 115.

12. I.A. Shirokov, Mesh construction algorithm based on TetGen for modeling the external flow around an axisymmetric model, Matem. Modelling, 2021, Vol. 13, No. 6, P. 1148 –1159.

13. TetGen: A quality tetrahedral mesh generator. http://tetgen.berlios.de/ (reference date 09.07.2021).

14. T. A. Kudryashova, S. V. Polyakov, and A. A. Sverdlin, Calculation of gas flow parameters around reentry vehicle, Math. Models Comput. Simul., 2009, Vol. 1, No. 4, P. 445 – 452.

15. K-100 System, Keldysh Institute of Applied Mathematics RAS, Moscow. https://www.kiam.ru/MVS/resourses/k100.html (reference date 09.07.2021).